12-2020

Investigating Mesospheric Mountain Waves and OH Temperature Dynamics Over Chile

David G. Soward
Utah State University

INVESTIGATING MESOSPHERIC MOUNTAIN WAVES AND OH TEMPERATURE DYNAMICS OVER CHILE.

by

David Soward

A thesis submitted in partial fulfillment
of the requirements for the degree

of

MASTER OF SCIENCE

in

Physics

Approved:

_____	_____
Mike Taylor, PhD. Major Professor	Ludger Scherliess, PhD. Committee Member
_____	
Jim Wheeler, PhD. Committee Member	

UTAH STATE UNIVERSITY
Logan, Utah

2020

Abstract

Atmospheric gravity waves (GW) occur throughout the atmosphere, propagating from copious sources in the lower atmosphere into the upper neutral atmosphere and ionosphere. There are many sources of GW, most of them are associated with strong weather disturbances which are highly transient in nature. Another source of GW are strong winds blowing over prominent mountains that generate mountain waves (MW.) An important property of all of these waves is that they propagate upwards, carrying large amounts of energy and momentum which can be deposited in the upper atmosphere as the waves saturate and break. The Andes Lidar Observatory (ALO) was established in 2009 with the primary goal to investigate the dynamics of the mesosphere over the massive Andes Mountains. The Mesospheric Temperature Mapper (MTM), developed by Utah State University, was installed at ALO (30°S, 70°W) in Chile in 2009 with two goals: a) to investigate novel temperature signatures of MW expected over the Andes and b) to obtain seasonal measurements of mesospheric temperature over this isolated region. The MTM obtains these data by measuring the OH airglow emission from which the temperature of the OH layer and the GW activity can be obtained. This study builds on previous work and continues to show the close correlation between the MTM temperature and simultaneous overpass measurements of mesospheric temperature made by the SABER instrument on the NASA TIMED satellite. The MTM consistently revealed a warm bias (~5K) over several years. The TIMED satellite was launched in 2001 and continues to provide near global atmospheric temperature data. Furthermore, an initial examination of MW events is presented. Important properties such as temperature perturbation and event structure are analyzed. These parameters will provide an initial overview of wave activity in the region.

1. Atmosphere and Gravity Wave Introduction

The atmosphere is divided into multiple layers starting with the troposphere at the Earth's surface and stretching in altitude into the exosphere at over 1000km. As the altitude increases the air density will decrease rapidly due to the gravity driven pressure gradient. Another important measurement of the atmosphere is the temperature. Temperature initially decreases as altitude increases, but in the stratosphere, thermosphere, and exosphere temperature increases. The temperature at the ground is primarily driven by the absorption of sunlight and decreases with altitude. At the tropopause the temperature reduces to a minimum and then starts to increase with altitude. This is due to absorption of ultraviolet light by the ozone layer in the overlying stratosphere. At the stratopause, the temperature reaches a second, more intense minimum. The mesosphere (~50-90km) lies above this region and is characterized by decreasing temperature reaching as low as 150K at the mesopause. Above this region lies the thermosphere which is characterized by continuous increase in temperature with altitude due to the absorption of extreme ultraviolet light by atomic oxygen. The ionosphere begins near 60km during the day and 100km at night.

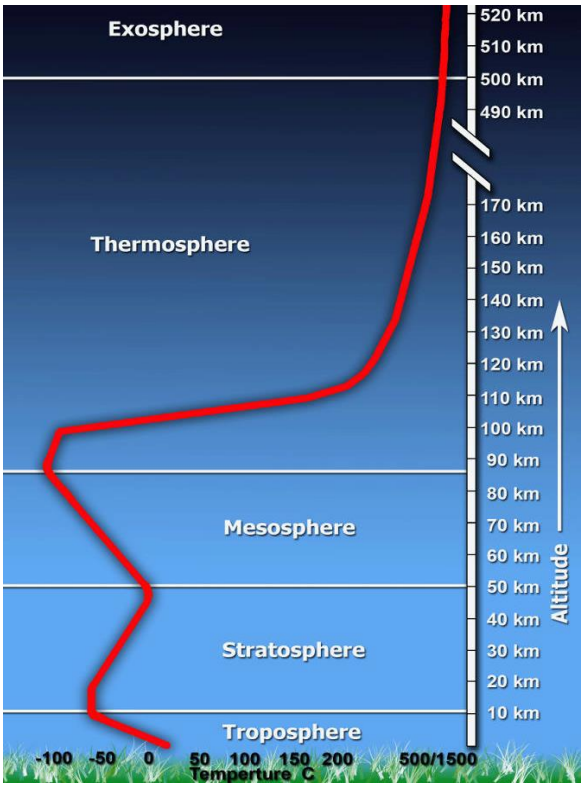

Figure 1: Temperature Profile of the Earth's atmosphere. Image courtesy Florida Atlantic University

An interesting occurrence that happens in the atmosphere are gravity waves. These waves can be compared with ripples in a body of water. They are formed as the water is displaced by an object being returned to equilibrium by gravity. GW can be formed by several sources in the lower atmosphere that include storms, volcanos, and strong winds blowing over mountain ranges. Any perturbation that causes air packets to be displaced vertically can produce GW. (Hines, 1960; Nappo, 2014). Waves can propagate upwards and transport energy and momentum into the upper atmosphere. As they travel upwards through the atmosphere, which is decreasing, exponentially, in density, their amplitude will increase. They will eventually break in the upper atmosphere which generally happens in the mesosphere (50-90km). This releases energy that impacts global circulation patterns which will affect climatology.

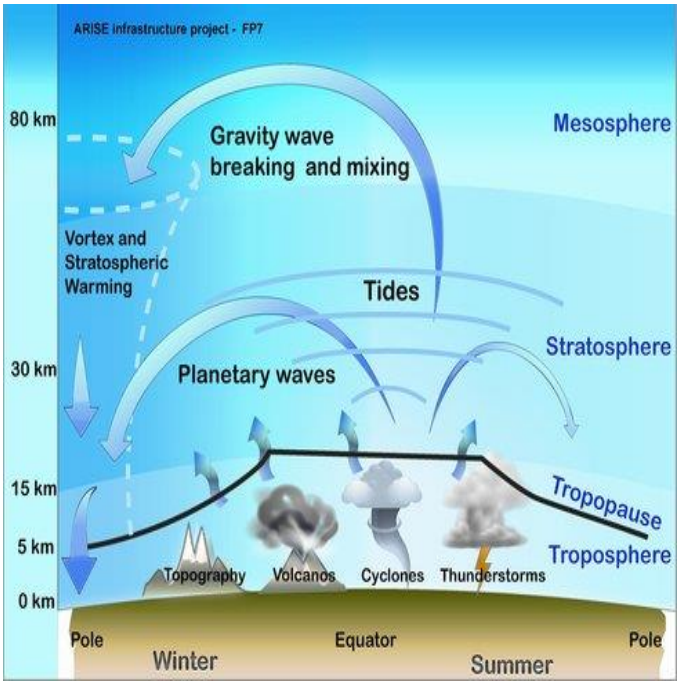

Figure 2: Diagram of atmospheric waves. Figure from Atmospheric Dynamic Research Infrastructure in Europe.

Generally, GW will freely propagate horizontality as they travel upwards away from their sources. However, one class of waves that will only travel vertically are mountain waves (MW.) These form as air is pushed upwards over a mountain range (Nappo, 2014).

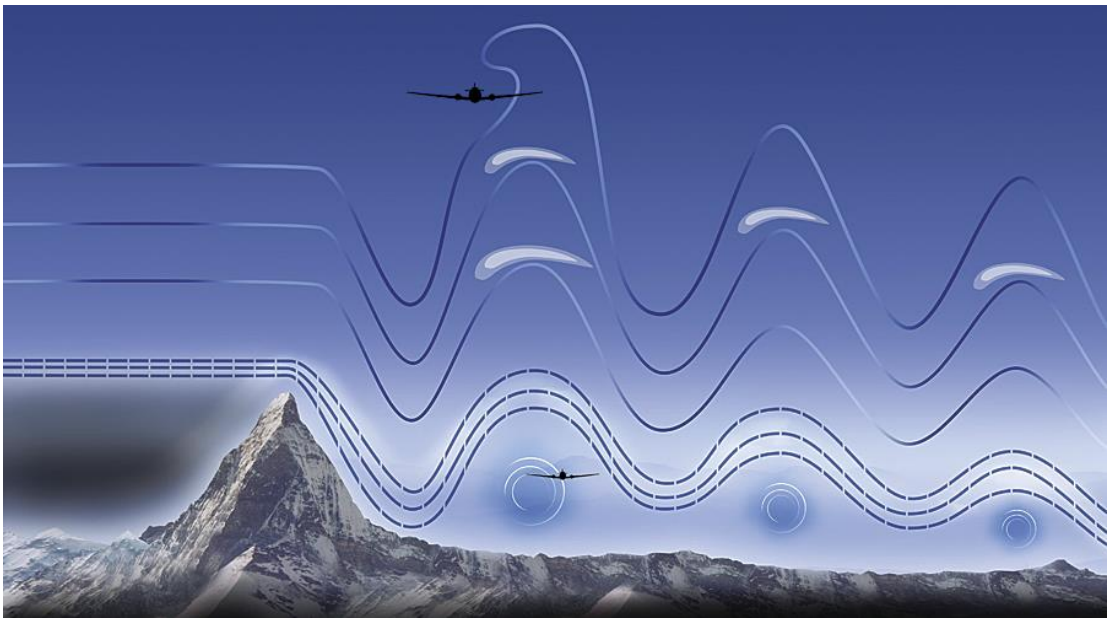

Figure 3: Generation, propagation, and structure of mountain waves. Sketch from ESRI.com

Like all gravity waves, mountain waves can impact energy transport in the upper atmosphere. Because of their broad range of scales and lifetimes, these MW are driven by two restoring forces in the atmosphere. The first is acoustic due to compressed air molecules that produce pressure gradients. The second force is due to gravity which acts to restore air parcel displacement to equilibrium. Together, these can create a spectrum of acoustic-gravity waves. (Hines et al.,1960) A special type of GW can occur when the intrinsic phase speed is equal and opposite to the background wind flow over an obstacle e.g. a mountain, generating stationary GW. These waves are frequently seen over prominent mountains when the winds and waves are in equal and opposite directions. This can be shown be letting $C_i = C_{Obs} - V$ where C_i is the intrinsic wave speed, C_{Obs} is the observed horizontal wave speed, and V is the background wind. Since MW are stationary in the horizontal direction, $C_{Obs} = 0$ which implies that $C_i = -V$. The vertical extension of the waves is also driven by this condition. These waves can produce severe turbulence for air traffic and reentering space craft, especially with the larger amplitudes they have at higher altitudes.

2. The Andes Lidar Observatory and Mesospheric Temperature Mapper

The Andes Lidar Observatory (ALO) was established in 2009 with the purpose of studying the dynamics of the upper atmosphere over the towering Andes mountain range. This facility contains many instruments that contribute to this task. As the name implies, the lidar is a key instrument that is used to sound the atmosphere. The sodium lidar can obtain measurements of Na density, temperature, and 3D wind velocities in the altitude range of 80-105 km. In addition to the sodium lidar system, the ALO also operates multiple all-sky imagers and a meteor wind radar which measures horizontal winds within the altitude range of 70-110km. Importantly, for this study, the ALO also houses the USU Mesospheric Temperature Mapper (MTM) instrument that has provided a significant amount of mesospheric temperature and GW image data over the Andes that are used in this study.

Figure 4 The Andes Lidar Observatory was established in 2009 with the primary goal to investigate the dynamics of the upper atmosphere over the massive Andes mountains. [Courtesy M.J. Taylor]

The MTM was designed and built at Utah State University (USU) and has been taking measurements since it was installed in Chile at Cerro Pachon (30.3°S, 70.7°W) during 2009. In operation it uses a cooled CCD imaging system to obtain band intensity and rotational temperature measurements of the OH (6,2) band which occurs in the near infrared region of the electromagnetic spectrum. This OH emission resides in a well-defined layer surrounding the Earth at a mean altitude of ~87km (layer thickness of ~6-8km full width half maximum) (Baker and Stair, 1988). The MTM field of view is ~90° allowing it to capture a broad range of small-scale GWs (horizontal wavelengths ~5-100km) in the mesosphere (Zhao et al., 2005).

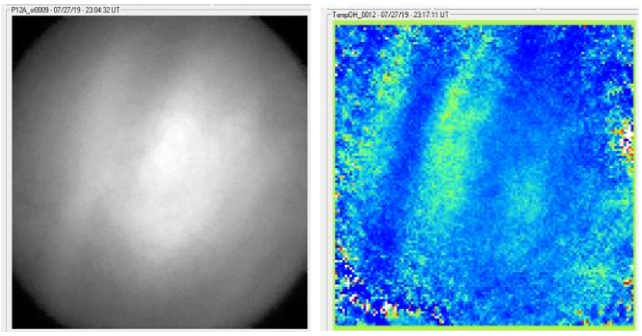

Figures 5a and 5b Example of processed ALO MTM imagery and temperature data from July 2019 where wave activity can be seen.

This study uses the MTM data in two different ways. The first is to measure the atmospheric temperature at the altitude of the airglow OH emission layer. These data are then used to establish frequent cross-calibrations by comparing with daily coincidence NASA TIMED satellite mesospheric temperature data. This comparison can then be used to investigate long term seasonal and year-to-year variability in mesospheric temperature. (Pugmire, 2018.) The second study uses the MTM two-dimensional image data to investigate the occurrence and properties of atmospheric GW and MW over Chile.

In operation, the OH band measurements are obtained using sequential observations of selected emission lines $P_1(2)$ and $P_1(4)$ which occur at 840 and 846.5 nm respectively. In addition, a background measurement is taken at 857 nm as well as a dark measurement are taken. A filter wheel is used to obtain these emission data using exposures of 60 seconds for each emission. (Taylor et al., 2001). The intensity ratio of these emissions provides an accurate estimate of the mesospheric OH rotational temperature which in turn is a good proxy of the atmosphere temperature at the OH layer altitude. In order to obtain high-quality measurements, the CCD temperature is kept at around -50°C to minimize thermal noise in the detector. Using this technique, the OH airglow layer can be used to study gravity wave activity and characteristics, including horizonal wavelength, phase velocity, temperature perturbation amplitude, occurrence, and duration.

Figure 6 Image of the MTM system [courtesy M.J. Taylor]. The MTM obtains these measurements by producing temperature maps of the OH airglow emission which are used to detect and measure GW events. Temperature and intensity maps are obtained approximately every three minutes.

3. SABER Instrument aboard TIMED

The Sounding of the Atmosphere using Broadband Emission Radiometry (SABER) is a space-based instrument and was launched on the Thermosphere, Ionosphere, Mesosphere, Energetics, and Dynamics (TIMED) satellite in 2001 with the purpose of obtaining data of the mesosphere and lower thermosphere (MLT) regions (Russel et al., 1999). SABER was built at the Space Dynamics Laboratory operated by USU. It has been gathering temperature data over the altitude range ~10-100 km on a global-scale since its launch. It is orbiting at approximately 625 km with an incline towards the equator of 74.1°.

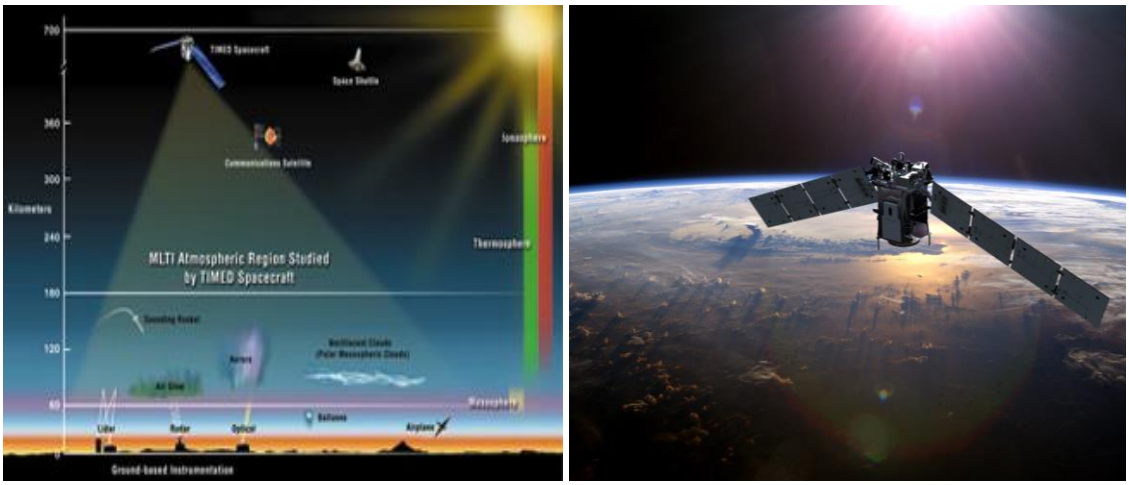

Figure 7a and 7b Image of SABER. Images from NASA and Johns Hopkins Applied Physics Laboratory

SABER also provides data regarding the energy, dynamics, and chemistry of the MLT regions. This infrared radiometer has a field of view of 2km vertical and 24km horizontal. It uses limb measurements of the CO2 profiles from Earth's lower atmosphere into the thermosphere (~10-100km) to measure kinetic temperature (Remsberg et al., 2008). In this investigation the SABER temperature profiles are used to compare with the MTM OH temperature measurements in the same observing region. This study provides a simple convenient way for cross-comparisons between the instruments, establishing confidence in their long-term measurements.

4. SABER and MTM Comparison

Early studies using a variety of ground-based temperature measurements, including MTM data from Maui, Hawaii, have shown that SABER is accurate to within ~5K in the Mesosphere and lower thermosphere region due to systematic and random errors (Remsberg et al., 2008). This study establishes SABER as a reliable reference for temperature comparison studies over the past ~two decades. For his 2018 dissertation, Dr. Jon Pugmire performed an in-depth analysis comparing the height-weighted temperature profiles of SABER centered at 87km with MTM OH temperature measurements obtained over an eight-year period (2009-2017.) The MTM data were all obtained at ALO, and as will be discussed later his results also establish a consistent offset of up to 5K, with a clear bias for the MTM warmer than SABER. In this study, two further years of ALO MTM data are investigated to build upon this prior result. An identical method of analysis was employed to identify measurements coincidences in these two data sets as discussed below.

The MTM uses a 1024 x 1024 pixel CCD array. For temperature measurements, the data were binned into 128 x 128 superpixels. The MTM superpixel field of view is 0.9 x 0.9 km. For this study, 5 x 5 super pixels were binned resulting in a 20.3 square km area centered on the zenith region at the altitude of the height weighted OH layer (Pugmire, 2018). In order to find coincidence

times that SABER overlaps with ALO some parameters must be first defined. SABER's orbit allows it to investigate ground comparisons over the latitude range 52°N to 52°S. A latitude-longitude box centered at ALO (30.3°S, 70.7°W) with selectable sizes of 5x5°, 10x10°, and 10x20° were used to define the sample region. SABER passes that intersect these regions constitute a potential event. In addition to these spatial limitations, a time frame of plus or minus six minutes for the event overpass time was used to ensure that SABER and the MTM data coincide during the same spatial and temporal range (see Figure 8 below.) Having a larger box size such as the 10x20° allows us to capture more coincidence SABER overpasses with MTM, since there is a greater area that it passes through. This contrasts with the smaller box size of the 5x5° which contains fewer, but more spatially localized events. Figure 8a shows coincidence MTM temperature measurement during a SABER overpass indicated by the highlighted red region. The strong nightly variability in temperature is evident, emphasizing the importance of short temporal sampling. Note the earlier SABER/MTM study from Maui, Hawaii also used a 10x20° latitude-longitude box size along with temporal range of 12 minutes (Remsberg et al., 2008). For reference, at ALO, a degree of latitude is ~111km and a degree of longitude is ~96km. Figure 8b shows the latitude versus longitude position of SABER tangent points during various overpasses in 2018 within a 10x20° box centered at ALO.

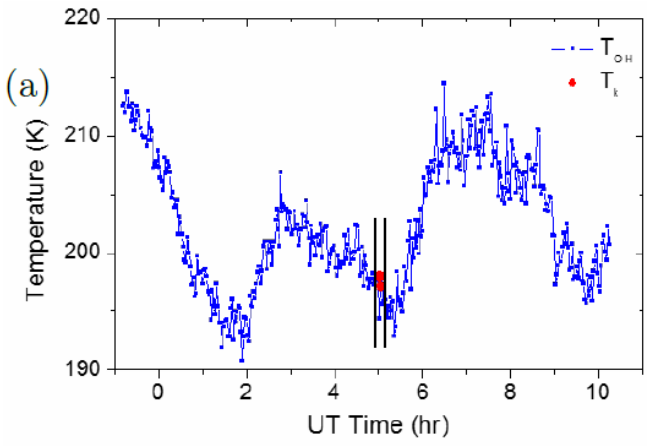

Figure 8a (above) Example of SABER/MTM coincidence May 22-23, 2012 at 5:00. The vertical black lines show the 12-minute coincidence limits using a spatial box size of 10x20°. Figure 8b (below) shows coincident overpasses for several different days, to illustrate SABER's geographic location with respect to ALO (orange dot), during 2018.

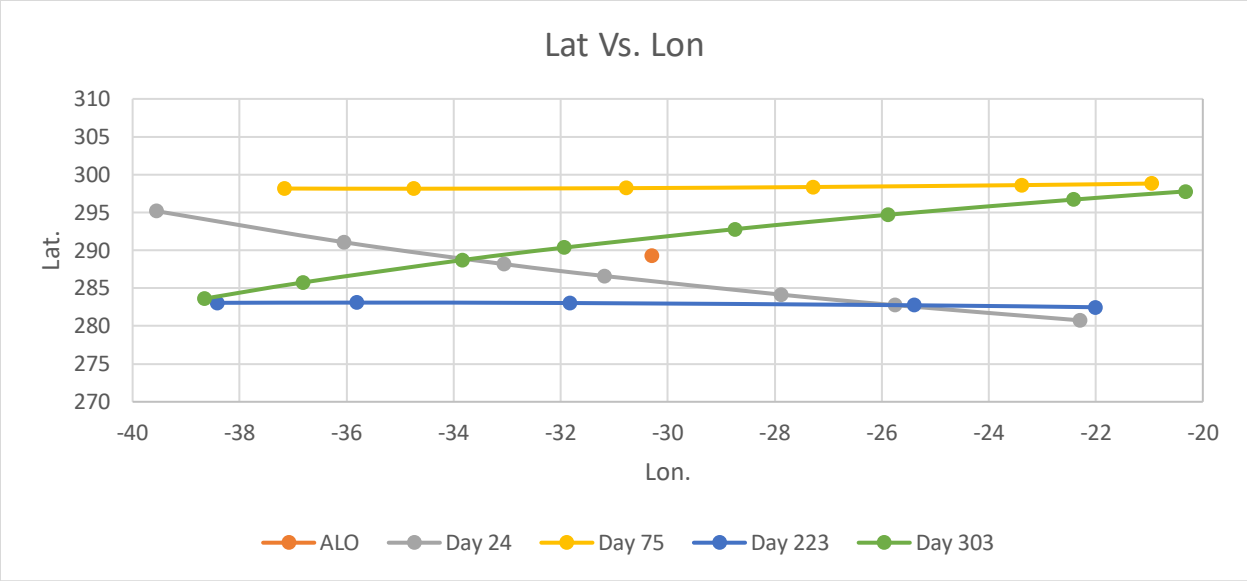

5. Results of Previous SABER and MTM Comparison at Chile

As previously discussed, the MTM and SABER comparison data from ALO revealed an offset of ~5K with the MTM being warmer than SABER from the distribution of events from 2009-2017. This is illustrated in Figure 9a which shows the results of his initial study using a 10x20° box size (Pugmire, 2018). Figure 9a plots the year versus SABER/MTM temperature measurements for eight consecutive years. SABER data are plotted in red and MTM in blue. To help emphasize the visual offset, a 30-day running mean was applied to both data sets. To further investigate the nature of the offset, Figure 9b plots the distribution of temperature differences revealing an offset of ~5K, and showing a Gaussian fit indicating the random nature of the errors as suggested by (Remsberg et al., 2008).

Previous MTM observations measured at Muai (Zhao et al., 2005) which took place prior to Pugmire's study all employed the 10x20° box size which captures several OH zenith and SABER average temperature measurements well in this volume. Figure 9c lists the derived offsets for the three different box sizes. They are all similar, establishing the continued use of the larger, 10x20°, box size for this follow-on study.

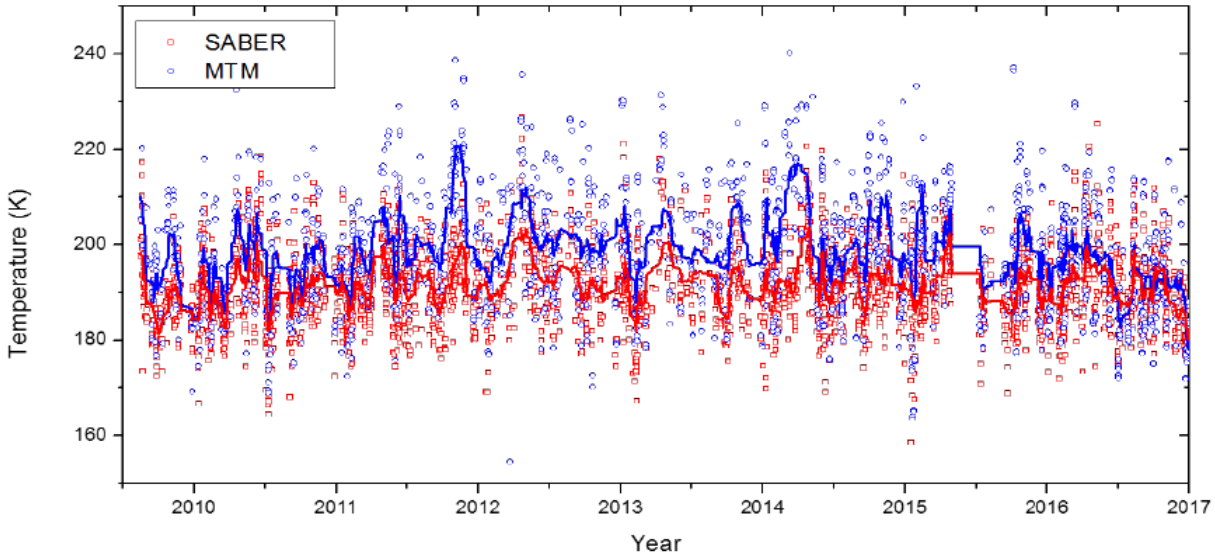

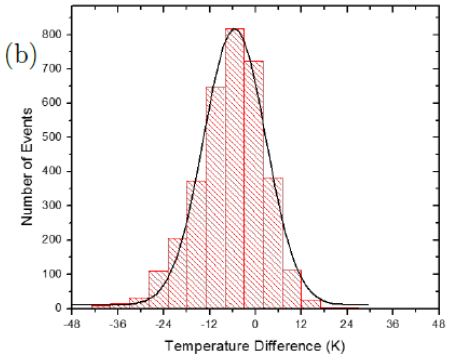

Spatial Criterion	Events	ΔT (K)
5°× 5°	394	−5.1
10°× 10°	1720	−5.2
10°× 20°	3465	−5.5

Figures 9a (top), 9b (bottom left), and 9c (bottom right.) Summary Results of SABER and MTM Comparison. (Table 4.1 and Figures 4.5 and 4.6 Pugmire, 2018)

6. New Results

The following results show a similar comparative analysis for the years of 2018 and 2019 conducted for this study.

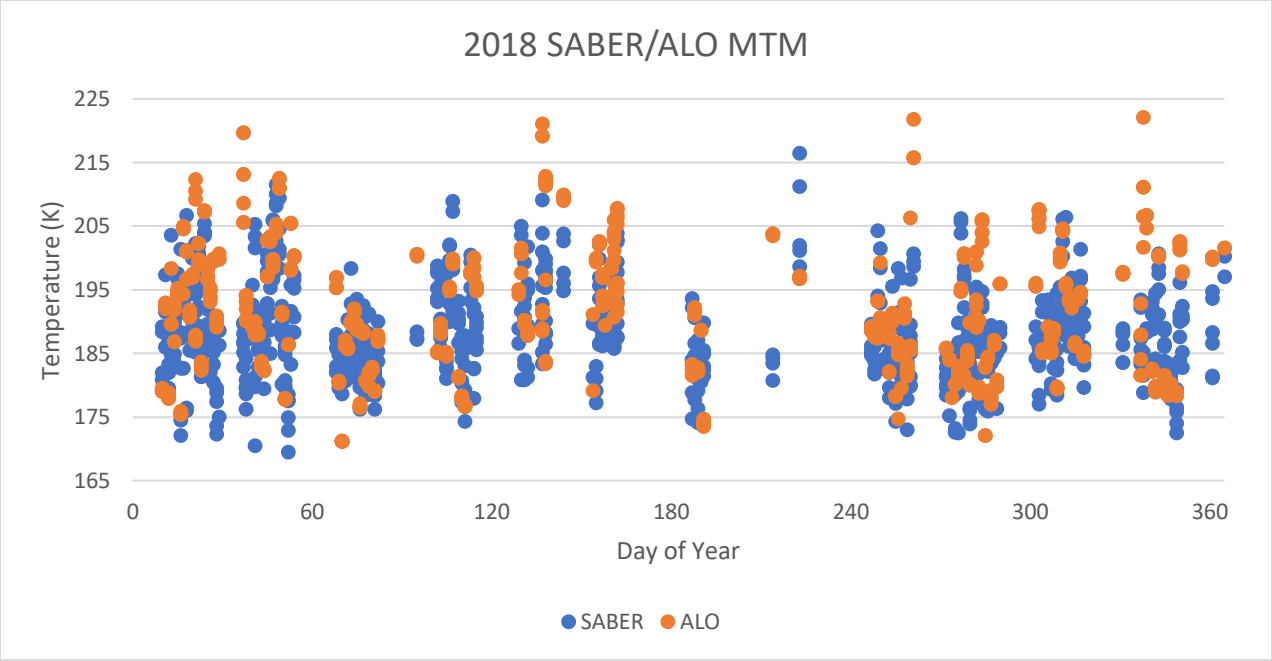

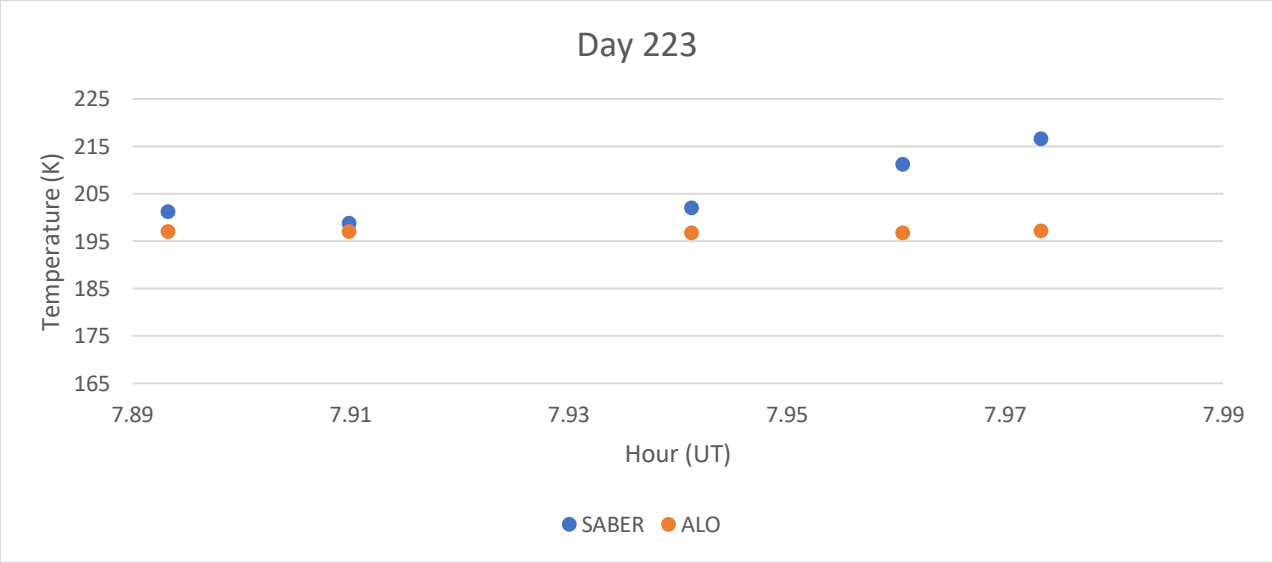

Figure 10a (top) and 10b (bottom) Plot comparing 895 coincidence SABER and MTM measurements for 10x20° in 2018 and a zoomed in view of Day 223. The temperature differences are listed in the table below

Box Size	SABER Yearly Mean	MTM Yearly Mean	Difference	Number of Events
10x20°	188.0K +/-7.3	191.0K +/- 11.4	3.0K	895
5x5°	186.9K +/- 6.1	190.2K +/- 8.9	5.1K	180

Figure 10a shows the comparison results for 2018 using a 10x20° spatial box. The figure plots day of year vs. SABER/MTM temperature measurements as in Figure 9a. Blue data points represent SABER measurements and orange points are for the ALO MTM. Each coincidence data

point has a corresponding pair of temperature readings from both SABER and MTM. Most nights have multiple coincidence events. On occasion, the MTM will provide readings that are about the same temperature value, so they will not all be visible on the yearly graph. An example of this is on day 223 which is investigated further in Figure 10b. The figure shows the time of day instead of day number to reveal that many data points can overlap, masking their appearance in Figure 10a. Figure 10b displays the mesospheric temperature measurements from SABER and the MTM during an approximately 6-minute overpass when 5 coincident measurements were made in a 10x20° sample region. A recurring feature of this data set in Figure 10a are the systematic gaps between clustered plot points. These known data gaps occur periodically for a few days each month and are due to the presence of light interference during full moon phase. Strong moonlight impacts the MTM data and measurements are not made for ~5 days dependent on the full moon. Figure 9 also has these gaps, but they are not obvious due to the compressed nature of eight years of data shown in this figure. Note the data are sparse from day 180 to 240 due to intermittent problems with the automatic data acquisition system. It is also wintertime in the southern hemisphere which can result in reduced observing conditions. The tabulated results indicate the MTM continues to show a warm bias, but a slightly smaller mean value of ~3K. These 2018 results are very similar to those observed during the previous eight years. Note that the plots for the smaller box sizes are included in Appendix A. To further investigate the 2018 results, Figures 11a and 11b compare the histogram distributions for the 5x5° box and 10x20° box.

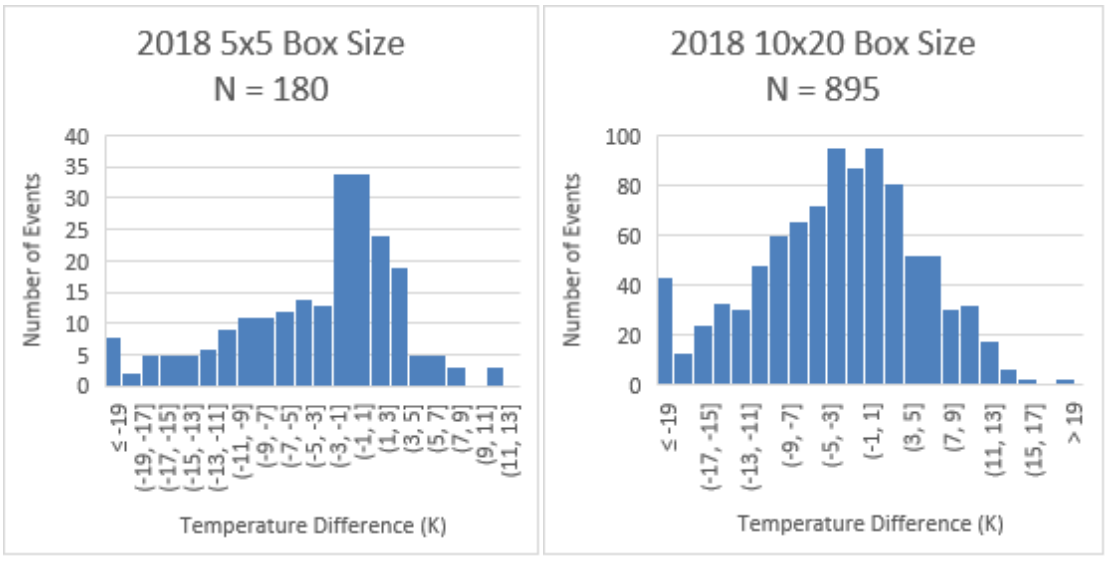

Figure 11a and 11b Are histogram plots comparing the 5x5° box size with the 10x20° box size temperature difference results, respectively

These two histograms reveal an important difference in the number of events and the measured shape of the distribution between the smallest and largest box size data sets. Although, all the measurements obtained in the 5x5° region are closer to the MTM's physical location, and should therefore be more accurate, the smaller area for the SABER measurements severely limits (N = 180) the number of coincident overpasses. In comparison the significantly larger number of

coincidences (N = 895) for the 10x20° box is due to the much larger sampling volume. The effect of this can be seen by the lack of symmetry in the 5x5° box size when compared with the 10x20° box results. These results indicate that in order to improve the statistical investigation of the temperature differences, using the 10x20° provides a larger data set that improves the shape of the distribution. For comparison, the distribution of Figure 9c was obtained using eight years of data (N = 3465).

It is important to note that the above data sets included coincidences during the entire night when the MTM was running. Due to this there is a period of ~2 hours at the start of the night that have interference from twilight, affecting the derived MTM temperature measurements. The impact of these twilight hours, on the number of events and the associated distributions are investigated below.

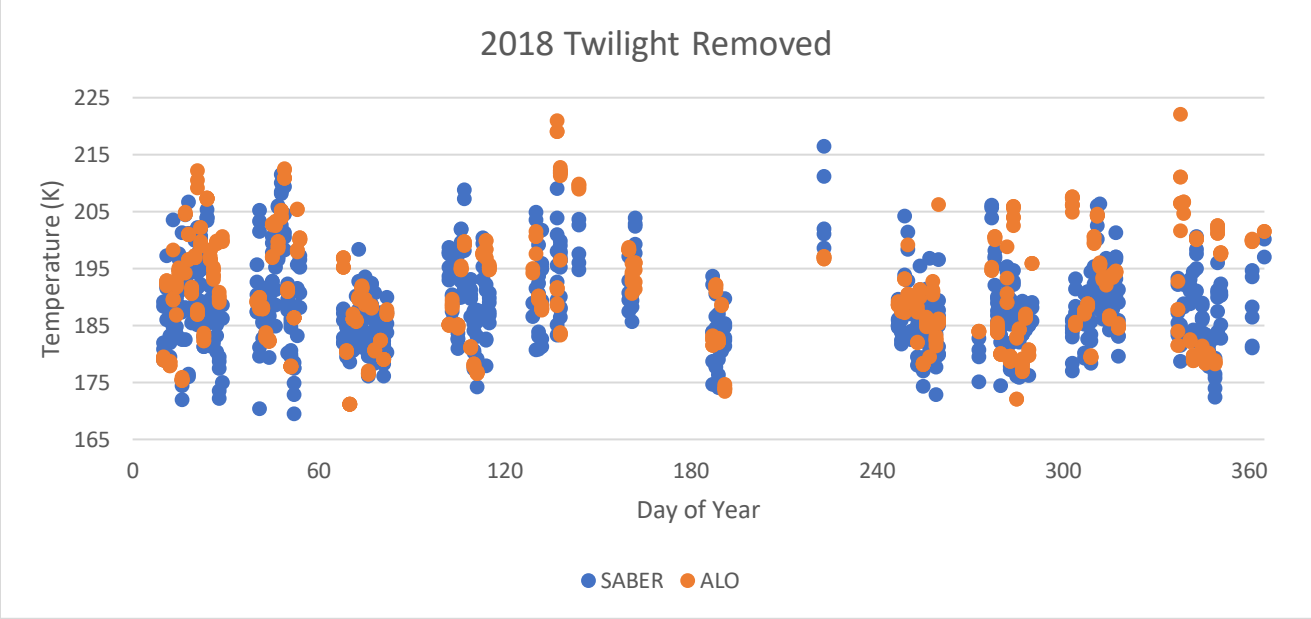

Data Set	SABER	MTM	Difference	Number of Events
Full	188.0K +/- 7.3	191.0K +/- 11.4	3.0K	895
Twilight Removed	188.6K +/- 7.5	190.9K +/- 11.5	2.3K	791

Figure 12 Comparison of coincidence SABER and MTM for 2018 with twilight's contributions removed

Removing the twilight hours from each day of the 2018 data slightly improved the correlation between the two instruments by 0.7K. The number of events decrease from 895 to 771 (16%) The effect of removing twilight is shown in the histograms below.

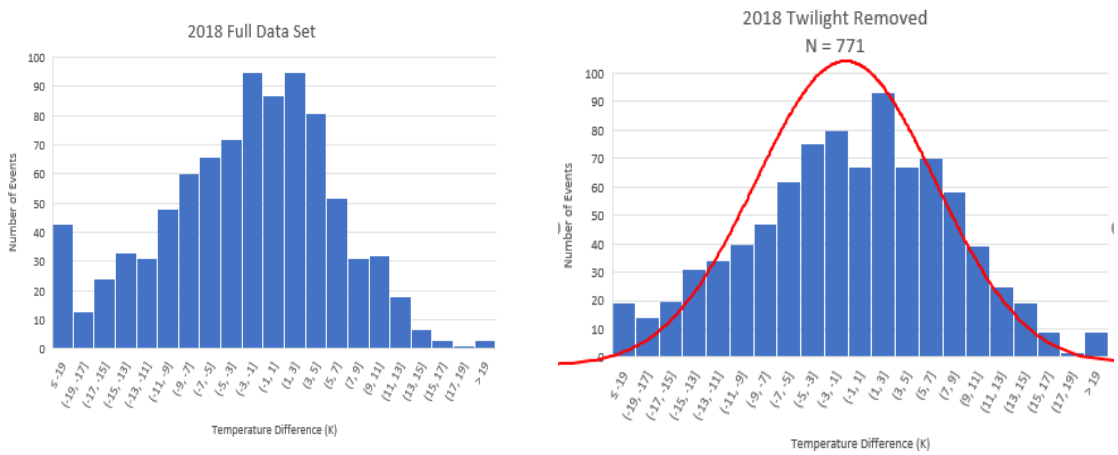

Figure 13a and 13b Histograms showing the frequency of temperature differences with both the full data set and with twilight removed for the 10x20° box

Figure 13b shows a distribution for the temperature differences as a result of removing twilight and outliers, a more-symmetric distribution is obtained. As before positive temperature differences indicate that the MTM is consistently warmer. The peak of the twilight removed data set also aligns with the measured temperature difference of 2.3K. This confirms the need to remove twilight hours, in addition to using a 10x20° spatial box. Removing the twilight hours will give a more accurate set of values.

7. 2019 Results

For direct comparison, the results are summarized for the following year 2019.

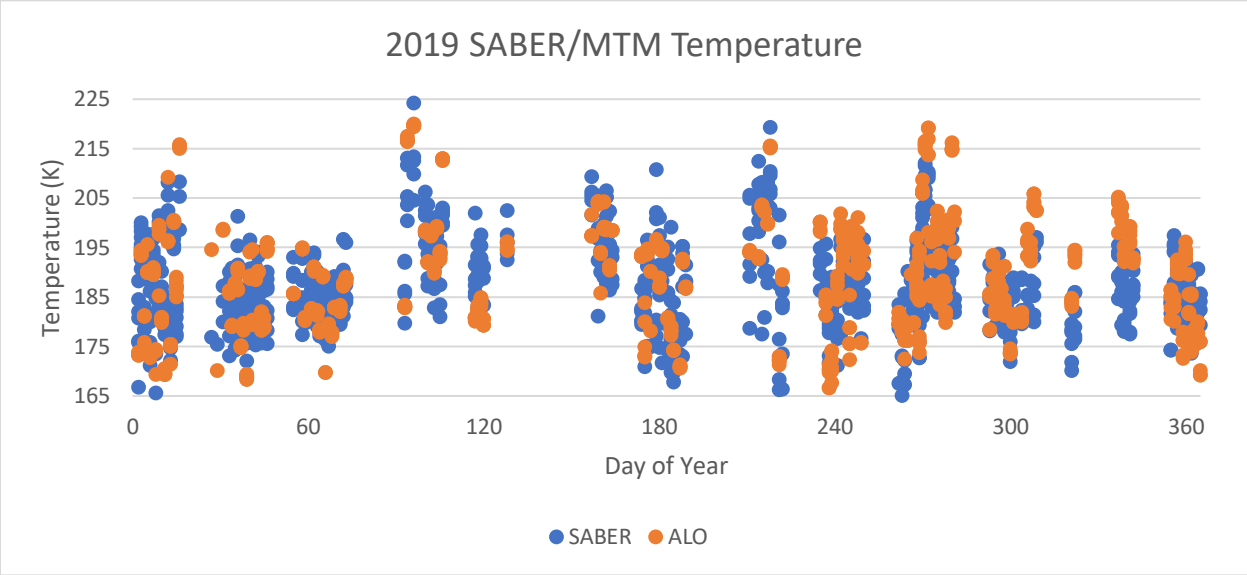

Year	SABER	MTM	Difference	Number of Events
2019	187.8K +/- 9.1	188.6K +/- 11.0	0.8K	880
2018	188.6K +/- 7.5	190.9K +/- 11.5	2.3K	791

Figure 14 Plot of Coincidence SABER and MTM for 2019 with twilight removed using a 10x20° box size

Figure 14 shows the same type of graph that is shown for the 2018 results. Once again, the MTM has a warmer mean temperature. As with the 2018 graph, the gaps in data are due to the presence of moonlight. Fortunately, there is not as large of a gap during the winter months as was present in 2018 although it is still a factor. Continuing to not have the two hours of twilight for each day in 2019 gives an extremely close mean temperature reading of 0.8K in favor of the MTM. This data set has coincident events relatively consistently throughout the entire year. This is an indication that SABER and the MTM continue to agree well with their respective temperature readings in 2019.

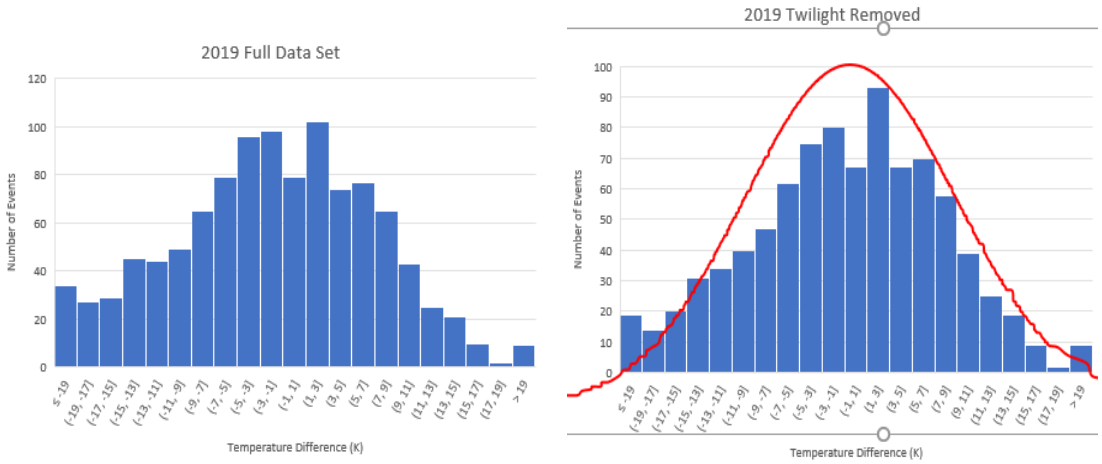

Figure 15 Histograms showing the frequency of temperature differences with both the full data set and with twilight removed

As seen in figure 15, twilight removal has an impact in the structure of the histogram, but it is not as pronounced as a difference as 2018 was. It still shows that having the twilight removed will produce better results.

8. 2018 and 2019 Combined Results

The combined results for both 2018 and 2019 are presented below. As before, the 10x20° box is employed along with twilight hours removed.

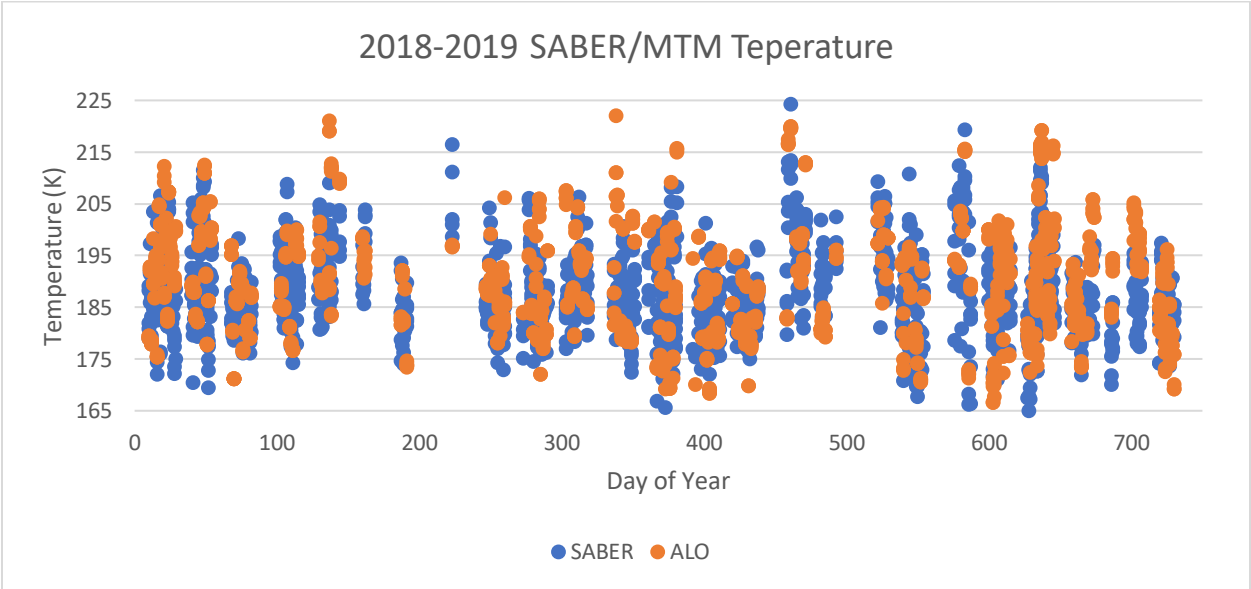

Year	SABER	MTM	Difference	Number of Events
2018	188.6K +/- 7.5	190.9K +/- 11.5	2.3K	791
2019	187.8K +/- 9.1	188.6K +/- 11.0	0.8K	880
2018-2019	188.1K +/- 9.6	189.7K +/- 11.2	1.6K	1651

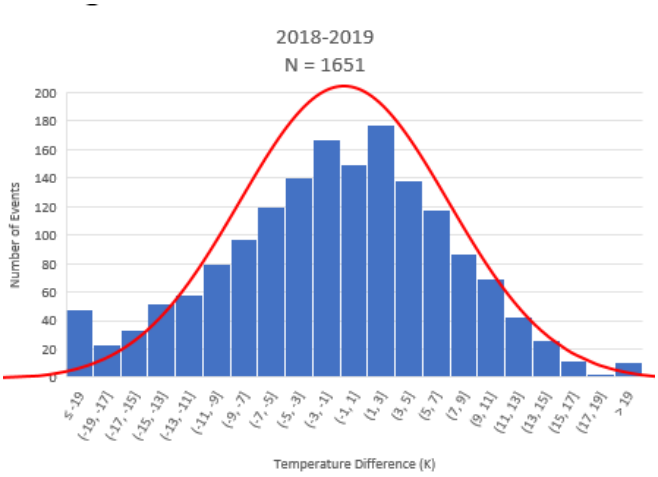

Figure 16a (top) Plot of Coincidence SABER and MTM for two years. Figure 16b (left) A histogram of temperature differences with a Gaussian distribution overlaid onto the histogram

Figure 16 indicates that there continues to be a high correlation between SABER and the MTM over the past two years. Combining both years increases the number of data points and helps fill in the scarcity of usable data during the winter months. The average temperature offset for both years (N =1651) is 1.6K with the MTM showing the warmer temperature reading. This is emphasized by the fitted Gaussian distribution.

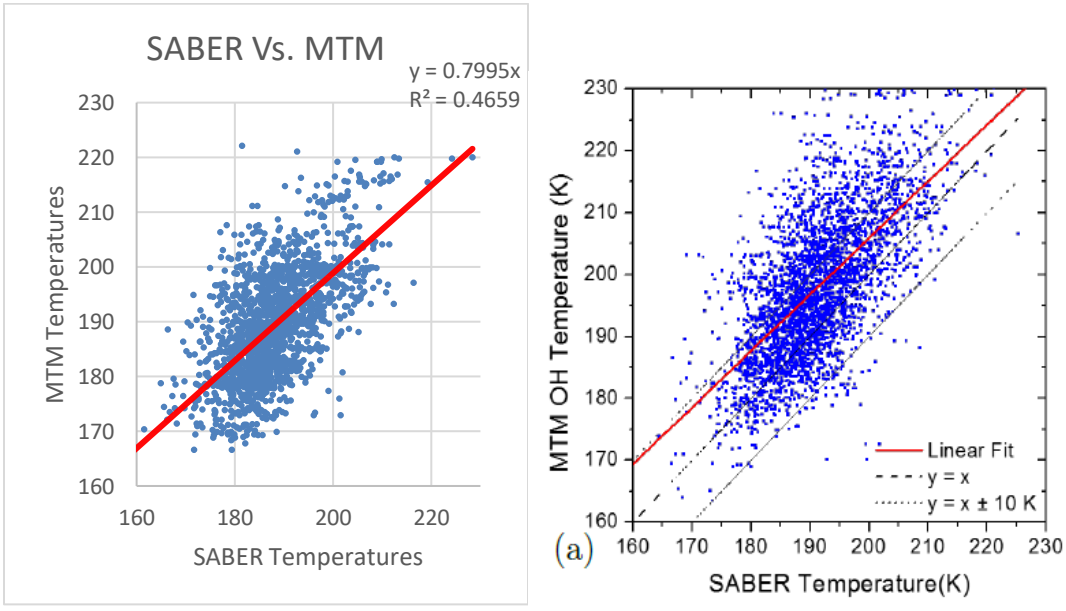

Figure 17a and 17b Plots of MTM Vs. SABER Temperature Measurements for 2018-2019 and 2009-2017 (From Figure 4.7b (Pugmire, 2018). Note the strong similarity of the overall shape and slopes over a broad range of temperatures.

Figure 17a and 17b shows the MTM temperature measurements plotted versus SABER temperature profiles. A similar plot is also shown for comparison (Pugmire, 2018). His slope is 0.9 over eight years of data, and the most recent two years of data have a slope of 0.8 The linear slopes indicate the consistency in temperature data readings by both of the instruments. The difference in the slope of the most recent measurements may be due to cloud interference. A previous mid-latitude study using The Ground Based Infrared P-Branch Spectrometer (GRIPS) located Wuppertal, Germany (7.2°E, 51.3°N) showed a slope of 0.99 over a period of three years, 2003-2005 using a 5x10° box size. (Oberheide et al., 2006). Together, these coordinated ground-based measurements, made using different instruments and techniques, over extended time intervals (2003-2019) continue to establish a high correlation with SABER over the past 1.5 decades and their importance for further correlative ground-based measurements with SABER.

9. Seasonal Comparison

Another way in which these data sets have been examined to investigate potential seasonal variability in the derived temperatures by the MTM and SABER. The section below provides a seasonal comparative study using the combined 2018-2019 data.

Figure 18 Plot MTM Vs. SABER temperature measurements for each month in 2018 and 2019 The data were combined to help improve the statistics of the winter-time measurements.

Month	Number of Events 2018	SABER 2018	ALO 2018	Temp. Diff. 2018	Number of Events 2019	SABER 2019	ALO 2019	Temp. Diff. 2019
January	132	189.3	195.7	6.4K	96	187.1	185.8	-1.3K
February	86	191.1	192.8	1.7K	105	184	184.7	0.7K
March	79	184.8	184.8	0K	65	185	183.3	1.7K
April	66	190.4	189.2	-1.2K	78	195.8	195.1	-0.7K
May	48	193.5	199	5.5K	5	196.5	195.2	1.3K
June	16	190.5	195.2	4.7K	80	191.7	193.7	2.0K
July	26	183.1	183.1	0K	39	184.1	182.8	-1.3K
August	12	194.2	192.2	-2.0K	78	189.9	190.6	0.7K
September	78	185.5	186.9	1.4K	114	188	189.3	1.3K
October	85	186.7	188.5	1.8K	93	187.6	188.9	1.3K
November	69	190.6	191.6	1.0K	32	184.7	195.2	10.5K
December	74	186.6	190.7	4.1K	95	184.9	187.1	2.2K

Figure 19 Values of the Monthly MTM Vs. SABER Temperature Measurements for 2018 and 2019

The above figures show the monthly plots and values for 2018 and 2019. In order to have a better understanding of any seasonal patterns in the temperature readings, the months have been broken up by season. For this study, winter is defined as May through August, spring is September and October, summer as November through February, and fall comprises March and April.

2018 Season	SABER	ALO	Temp Diff.	Number of Events
Winter	190.3 +/- 6.1	192.4 +/- 5.5	2.1	102
Spring	186.1 +/- 0.3	187.7 +/- 0.9	1.6	163
Summer	189.4 +/- 1.3	192.7 +/- 2.0	3.3	361
Fall	187.6 +/- 7.6	187.0 +/- 3.8	-0.6	145

2019 Season	SABER	ALO	Temp Diff.	Number of Events
Winter	190.6 +/- 5.5	190.6 +/- 6.0	0	202
Spring	187.8 +/- 0.3	189.1 +/- 1.1	1.3	207
Summer	185.2 +/- 4.8	188.2 +/- 2.2	3.0	328
Fall	190.4 +/- 8.4	189.2 +/- 3.1	-1.2	143

Figure 20a and 20b Values of the mean temperatures and differences for the Seasonal comparison MTM Vs. SABER Temperature Measurements for 2018 and 2019, respectively

Figures 20a and 20b show that there is good correlation throughout the year between both instrument's temperature measurements. Although the MTM observes a higher average yearly temperature (1.6K See Figure 16) which is true for winter and spring of both years. However, the table shows that for both years, SABER exhibited a reversal in the average seasonal temperature difference to become slightly warmer during the fall. While this small difference does not significantly impact the yearly comparison, it is an interesting feature to further investigate possibly using continued temperature measurements at ALO or from other sites at different latitudes.

10. Individual Wave Events Observed by the MTM

A second part of this report presents the results of a detailed visual study of the MTM intensity and temperature image data focusing on the winter months when GWs generated by strong eastward winds blowing over the Andes Mountains enable them to propagate to high altitudes. Previous studies from Argentina (Smith et al., 2009) have detected stationary GW in the mesospheric airglow emissions during the winter months. The MTM is able to measure the structure and brightness of these waves as well as their temperature perturbations. Images and temperature maps are produced by the MTM located at ALO. This image data includes stars in the image that are easily detected and removed (Garcia et al., 1997). The images are then calibrated, flat-fielded and projected into the geographic grid centered over Cerro Pachon. The temperature maps are then derived from the ratio of sequential $P_1(2)$ and $P_1(4)$ images. (Taylor et al., 2001) This creates geographic maps of the GWs at the ~87km level extending over an area of 200x200km in the OH intensity and temperature field. Unfortunately, observations during the winter months (May-August) are limited due to variable weather as noted in Figure 10. From a

study of eight months of wintertime data during 2018-2019, observations indicating quasi-stationary GW were obtained on ~7-15 nights of variable duration. They were categorized by their orientation approximately parallel to the Andes and observed low phase speeds. Example events are presented here for comparison.

Event Date	Observation Period
May 10th, 2018	2 Hours 45 Minutes
June 28th, 2019	15 Minutes
July 24th, 2019	45 Minutes

Figure 21 A table of three highlighted wave events obtained from ALO MTM

Figure 21 tabulates three distinct events that are examined in the following section. Refer to the appendix for a larger list of MW events that were observed during winter 2018-2019.

Event #1: May 10th, 2018:

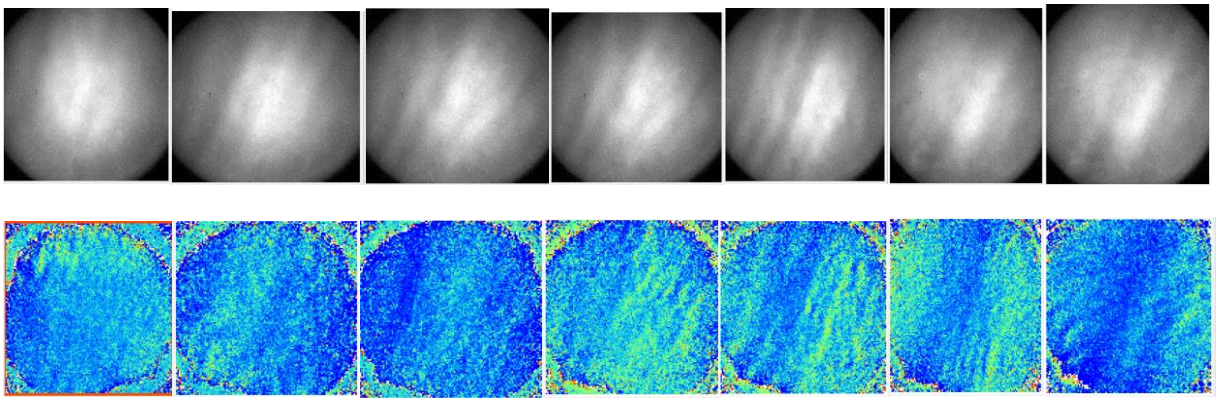

Figure 22 The top row show the OH band intensity images while the bottom row show the derived temperature maps for May 10-11, 2018 from 23:20-02:42 UT at ~20 minute intervals.

Figure 22 shows the evolution of a GW event that takes place on May 10th-11th, 2018 (images are shown in regular intervals.) In the top row, wave activity can be seen in the OH band intensity. The bottom row shows the corresponding derived temperature maps where "peaks and troughs" in temperature are generated by the waves. This particular event was observed continuously for over seven hours and exhibited large standing waves with a near north-south alignment, characterizing it as a potential MW event. These waves persisted throughout this event. These images are snapshots of the event taken at 20-minute intervals and extend from 23:22 to 02:42 UT. The MW created a temperature perturbation of ~19K (193K in the trough and 212K at the peak.) The measured wavelength for the larger wave event was ~18km. Examination of the evolution of this event shows the development of much shorter waves parallel to the larger scale event. These smaller waves grew significantly during the course of this event. They exhibited

horizontal wavelengths of ~9km, and are likely due to the development of strong instabilities associated with the MW breaking in the mesopause region (Hecht et al.2014)

Event #2: June 28th, 2019:

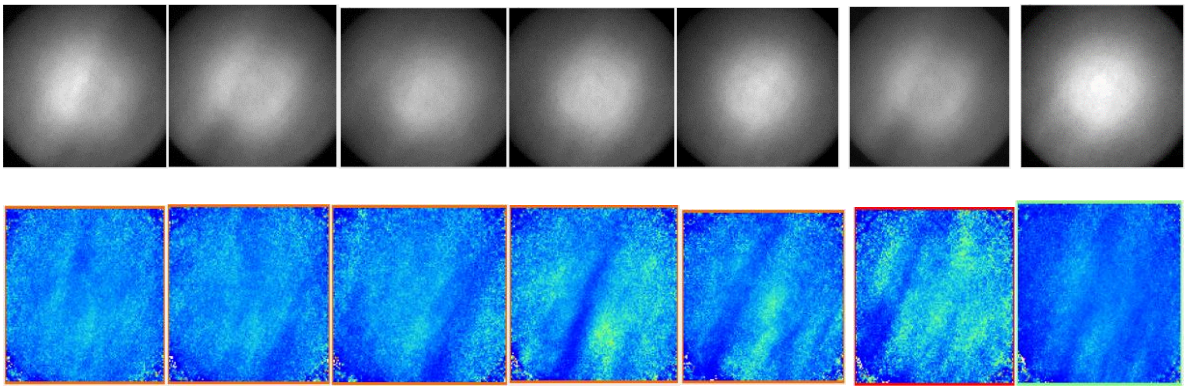

Figure 23: The same format as Figure 22, but for June 28, 2019, and was observed from 23:17 to 23:32 UT. Data were taken ~2-minute intervals. After this time, the data were impacted by cloud interference.

This event was observed for only a short time (15 minutes.) The images shown in Figure 23 were taken at high cadence, ~2 minutes intervals starting at 23:17UT until 23:32UT. Initially not much details of the event are visible, but during this image sequence, a wave event of similar orientation to event #1was observed as the second event progressed. The prominent structures display a horizontal wavelength of about 35km and produced a temperature perturbation of ~23K (peak 190K to trough 167K). This event did not show strong signatures of instabilities development during this limited time period.

Event #3: July 24th, 2019:

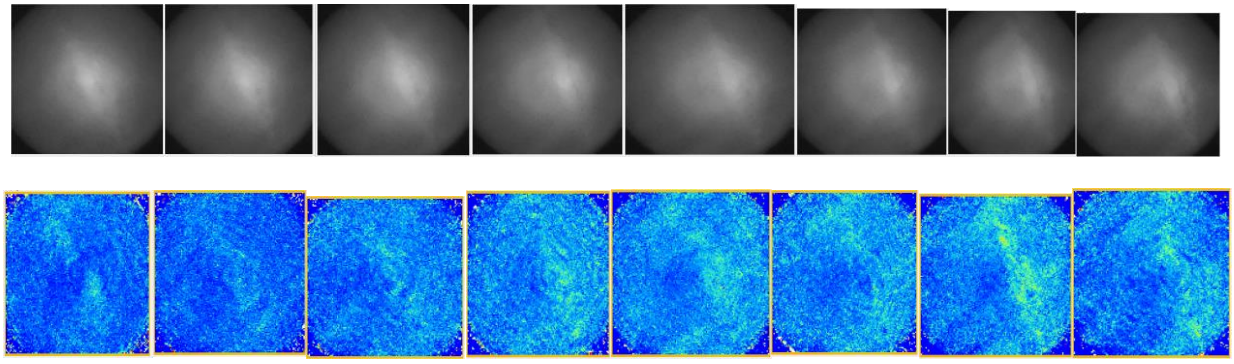

Figure 24: The same format as Figures 22 and 23, but for July 24th-25th, 2019 over 5-minute intervals. Wave structures are quite different, containing large numbers of smaller scale circular type waves moving across the field of view, illustrating the night to night variability of the data.

Figure 24 shows a different type of wave event observed during the night of July 24th and into the morning of the 25th. Unlike the previous wave events that exhibited slowly evolving

structures over the course of the night. Instead, these images contain large number of smaller scale circular type waves moving across the field of view. The event duration is also, significantly shorter, from 2:40 to 3:12. The horizontal wavelengths measured are ~11km.

Event	Observed Duration	Temperature Perturbation	Horizontal Wavelength
1 MW breaking	2 Hours 45 Minutes	19K	17.8km, 8.9km
2 MW	17 Minutes	23K	35km
3 Circular GW	45 Minutes	Not Measured	11.3km

Figure 25: A table that summarizes important parameters of the three presented wave events

In summary, Figure 25 compares examples of three wave events that were described in the previous section helping establish the existence and properties of MW activity over the Andes. They are all able to transport energy and momentum into the upper atmosphere. As evidenced by these data, waves can have a localized impact on temperature by up to 20k. Further detailed analysis of these and other wave events such as those listed in the appendix, together with available radar and lidar data will enable the investigation of the impact of waves on the mesosphere and lower thermosphere, providing a more accurate picture of wave variability within earth's upper atmosphere.

Appendix:

In this appendix, further details of the MTM/SABER comparisons are presented for further investigation.

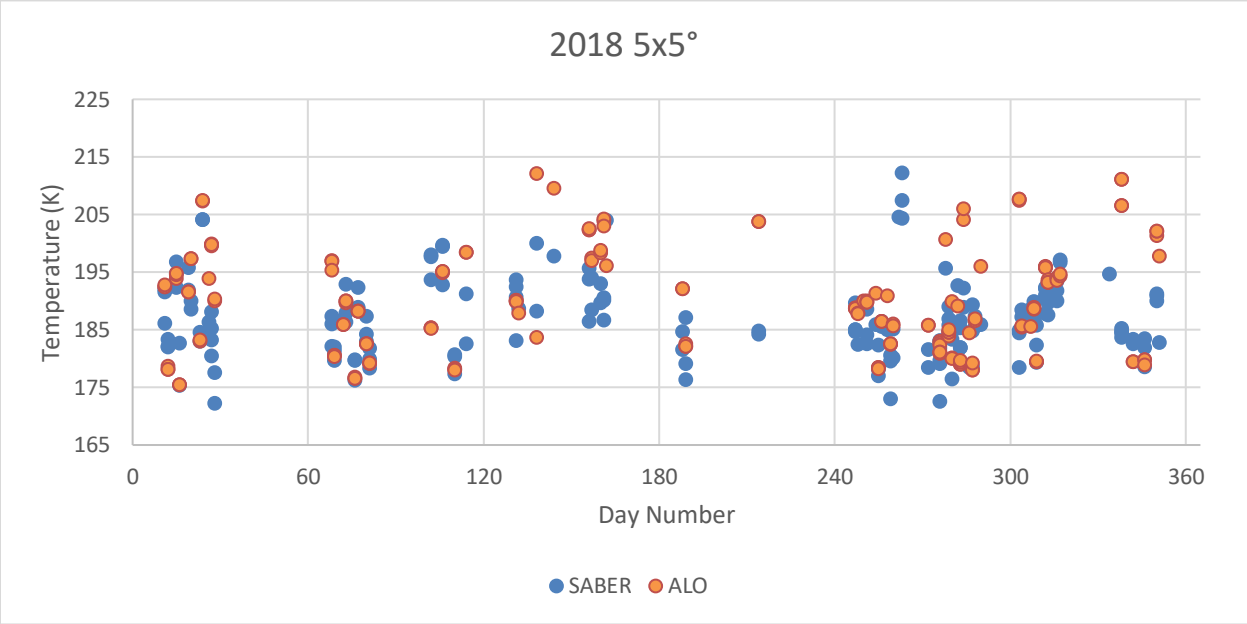

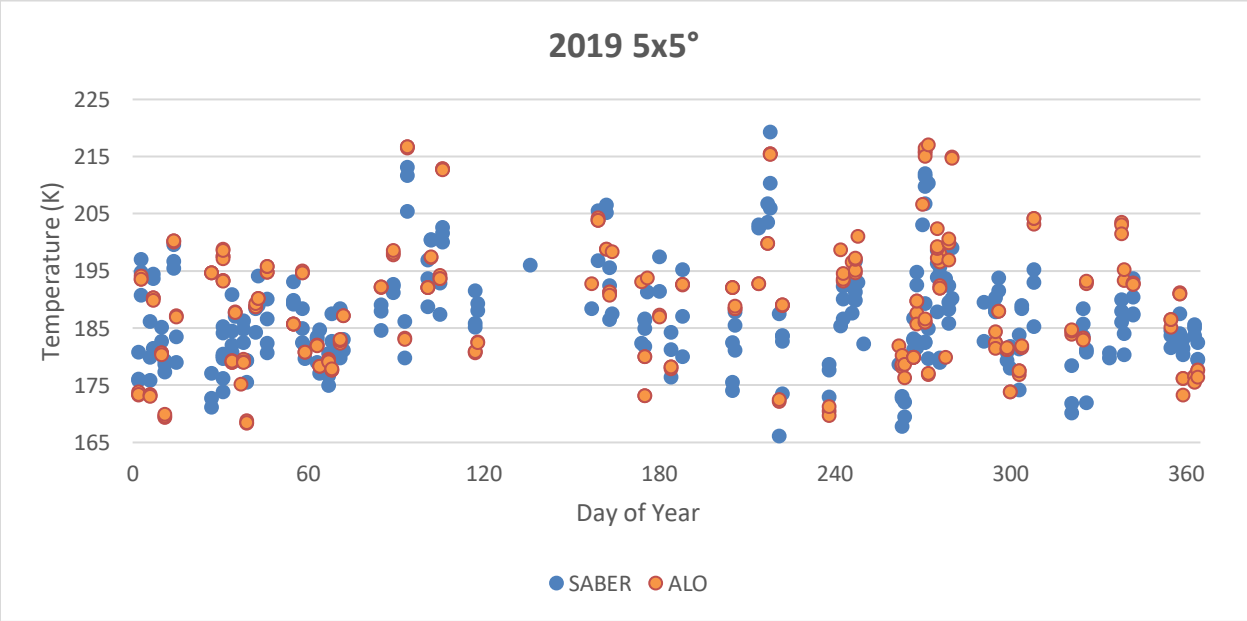

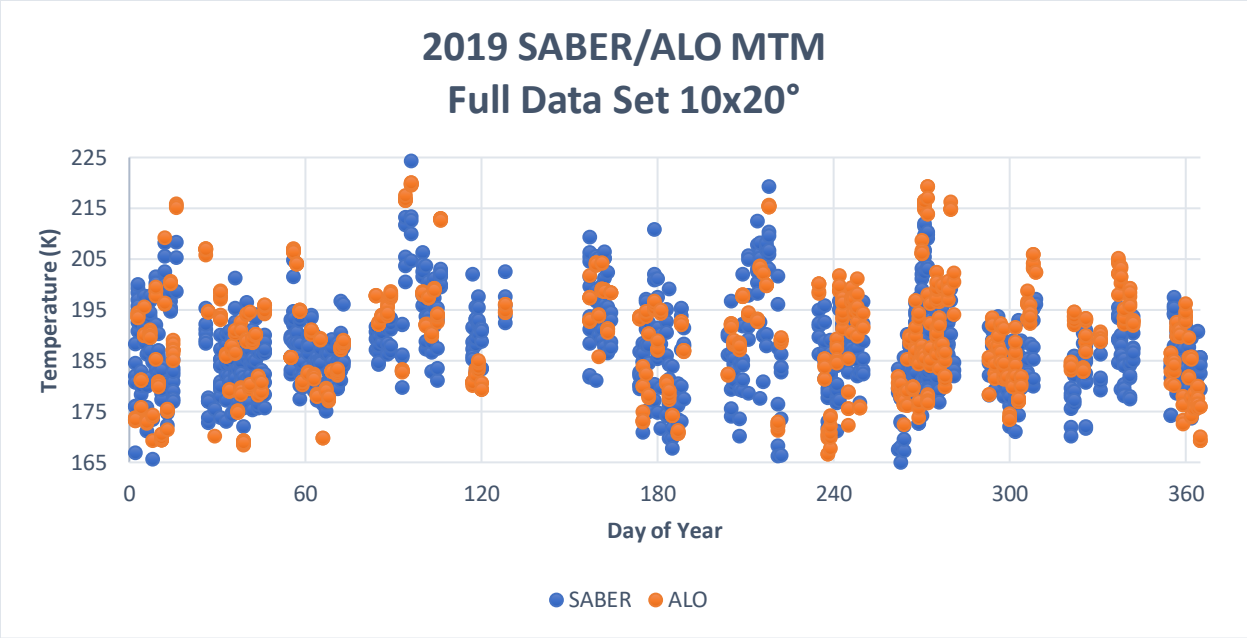

SABER	MTM	Difference	Number of Events
187.3K	189.7K	2.4K	1073

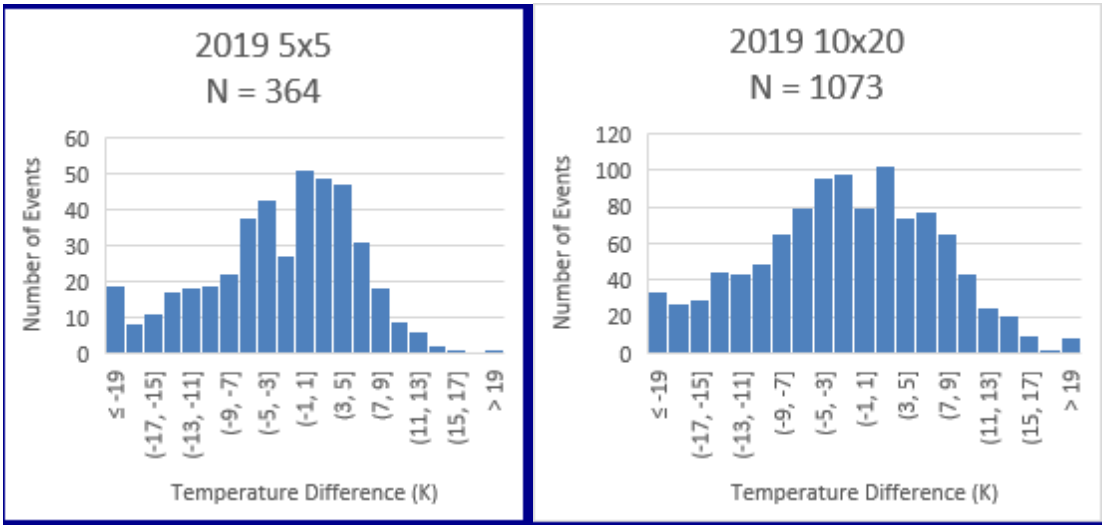

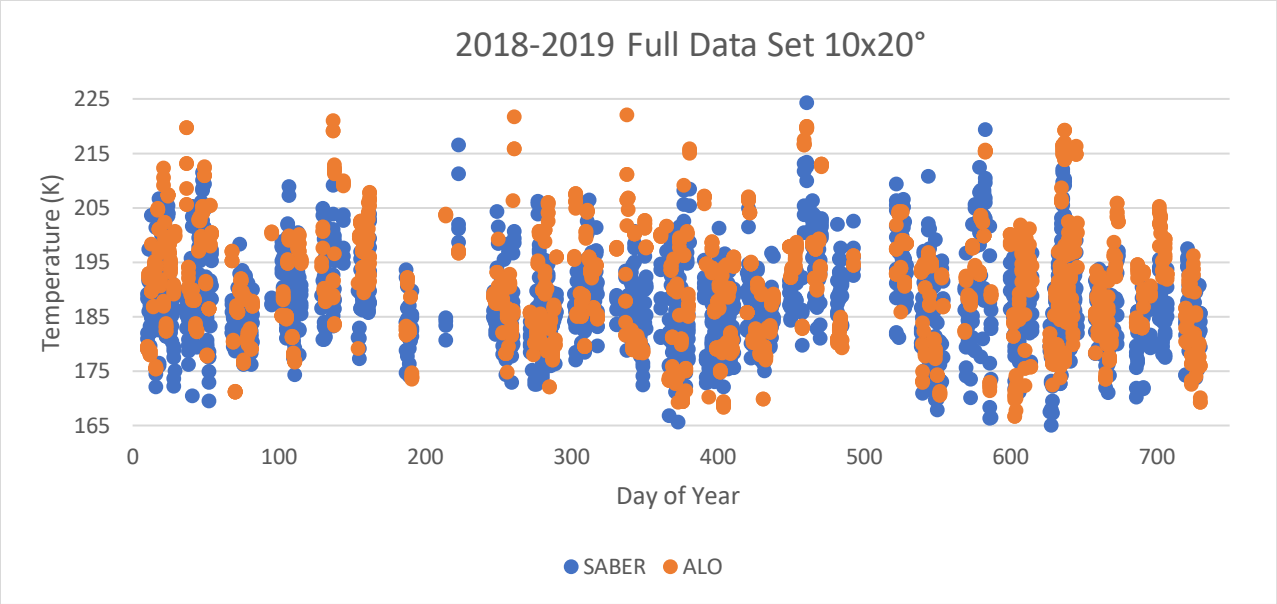

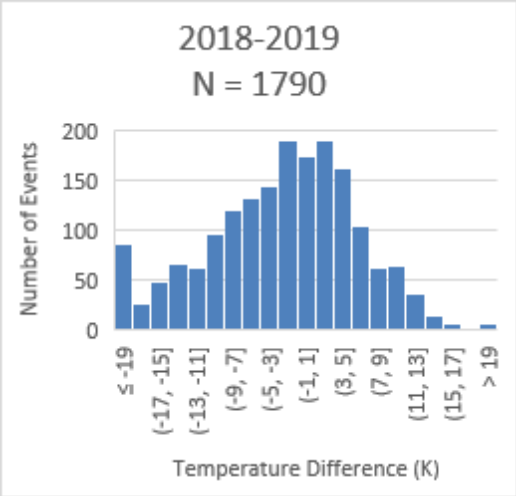

Further information is provided on more GW events observed by the MTM

Event Date	Duration
May 10th, 2018	2 Hours 45 Minutes
July 28th, 2019	36 Minutes
July 27th, 2019	15 Minutes
July 25th, 2019	2 Hours
June 24th, 2019	50 Minutes
January 19th, 2019	46 Minutes
July 29th, 2019	23 Minutes
July 24th, 2019	1 Hour 45 minutes

References

Baker, D. J., and A. Stair Jr (1988), Rocket measurements of the altitude distributions of the hydroxyl airglow, Phys. Scripta,37(4), 611.

Garcia, F., M. J. Taylor, and M. Kelley (1997), Two-dimensional spectral analysis of mesospheric airglow image data, Applied optics, 36 (29), 7374–7385.

Hecht, J., K. Wan, L. Gelinas, D. C. Fritts, R. Walterscheid, R. Rudy, A. Liu, S. J.Franke, F. Vargas, P.-D. Pautet, et al. (2014), The life cycle of instability features measured from the Andes Lidar Observatory over Cerro Pachon on 24 march 2012, J. Geophys. Res. Atmos.,119(14), 8872–8898.

Hines, C. (1960), Internal atmospheric gravity waves at ionospheric heights, Can. J.Phys.,38(11), 1441–1481.

Oberheide, J., D. Offermann, J. Russell, and M. Mlynczak (2006), Intercomparison of kinetic temperature from 15µm CO2limb emissions and OH*(3, 1) rotational temperature in nearly coincident air masses: SABER, GRIPS, Geophys. Res. Lett.,33(14).

Nappo, C. (2002), An Introduction to Atmospheric Gravity Waves, no. v. 1 in An Introduction to Atmospheric Gravity Waves, Academic Press.

Pugmire, Jonathan Rich, "Mesospheric Gravity Wave Climatology and Variances Over the Andes Mountains" (2018). *All Graduate Theses and Dissertations*. 7387

Remsberg, E., B. Marshall, M. Garcia-Comas, D. Krueger, G. Lingenfelser, J. Martin-Torres, M. Mlynczak, J. Russell, A. Smith, Y. Zhao, et al. (2008), Assessment of the quality of the version 1.07 temperature-versus-pressure profiles of the middle atmosphere from TIMED/SABER,J. Geophys. Res. Atmos. (1984–2012),113(D17).

Russell III, James M., Martin G. Mlynczak, and Larry L. Gordley, Overview of the Sounding of the Atmosphere Using Broadband Emission Radiometry (SABER) experiment for the Thermosphere-Ionsphere-Mesosphere Energetics and Dynamics (TIMED) mission, Proc. SPIE 2266, 406-415, doi:10.1117/12.187579, 1994.

Russell III, J. M., M. G. Mlynczak, L. L. Gordley, J. J. Tansock Jr, and R. W.Esplin (1999), Overview of the SABER experiment and preliminary calibration results, in SPIE's International Symposium on Optical Science, Engineering, and Instrumentation, pp. 277–288, International Society for Optics and Photonics.

Smith, S., J. Baumgardner, and M. Mendillo (2009), Evidence of mesospheric gravity-waves generated by orographic forcing in the troposphere, Geophys. Res. Lett.,36(8).

Taylor, M. J., L. Gardner, and W. Pendleton Jr (2001), Long-period wave signatures in mesospheric OH Meinel (6,2) band intensity and rotational temperature at mid-latitudes, Advances in Space Research,27(6), 1171–1179.

von Savigny, C., K.-U. Eichmann, E. Llewellyn, H. Bovensmann, J. Burrows, M. Bittner, K. Höppner, D. Offermann, M. J. Taylor, Y. Zhao, et al. (2004), First near-global retrievals of OH rotational temperatures from satellite-based Meinel band emission measurements, Geophys. Res. Lett.,31(15).

Zhao Y, Taylor MJ, Chu X. Comparison of simultaneous Na lidar and mesospheric nightglow temperature measurements and the effects of tides on the emission layer heights. *Journal of Geophysical Research Atmospheres*. 2005;110(D9)